

**PUSH THE LIMITS
OF SENSITIVITY**

CellStream™ flow cytometers

[Learn More](#)



The Journal of
Immunology

Structural Basis for the Function of Complement Component C4 within the Classical and Lectin Pathways of Complement

This information is current as of September 2, 2018.

Sofia Mortensen, Rune T. Kidmose, Steen V. Petersen, Ágnes Szilágyi, Zoltan Prohászka and Gregers R. Andersen

J Immunol 2015; 194:5488-5496; Prepublished online 24 April 2015;
doi: 10.4049/jimmunol.1500087
<http://www.jimmunol.org/content/194/11/5488>

Supplementary Material <http://www.jimmunol.org/content/suppl/2015/04/24/jimmunol.1500087.DCSupplemental>

References This article **cites 48 articles**, 19 of which you can access for free at:
<http://www.jimmunol.org/content/194/11/5488.full#ref-list-1>

Why *The JI*? Submit online.

- **Rapid Reviews! 30 days*** from submission to initial decision
- **No Triage!** Every submission reviewed by practicing scientists
- **Fast Publication!** 4 weeks from acceptance to publication

**average*

Subscription Information about subscribing to *The Journal of Immunology* is online at:
<http://jimmunol.org/subscription>

Permissions Submit copyright permission requests at:
<http://www.aai.org/About/Publications/JI/copyright.html>

Email Alerts Receive free email-alerts when new articles cite this article. Sign up at:
<http://jimmunol.org/alerts>

The Journal of Immunology is published twice each month by
The American Association of Immunologists, Inc.,
1451 Rockville Pike, Suite 650, Rockville, MD 20852
Copyright © 2015 by The American Association of
Immunologists, Inc. All rights reserved.
Print ISSN: 0022-1767 Online ISSN: 1550-6606.



Structural Basis for the Function of Complement Component C4 within the Classical and Lectin Pathways of Complement

Sofia Mortensen,* Rune T. Kidmose,* Steen V. Petersen,[†] Ágnes Szilágyi,[‡]
Zoltan Prohászka,[‡] and Gregers R. Andersen*

Complement component C4 is a central protein in the classical and lectin pathways within the complement system. During activation of complement, its major fragment C4b becomes covalently attached to the surface of pathogens and altered self-tissue, where it acts as an opsonin marking the surface for removal. Moreover, C4b provides a platform for assembly of the proteolytically active convertases that mediate downstream complement activation by cleavage of C3 and C5. In this article, we present the crystal and solution structures of the 195-kDa C4b. Our results provide the molecular details of the rearrangement accompanying C4 cleavage and suggest intramolecular flexibility of C4b. The conformations of C4b and its paralogue C3b are shown to be remarkably conserved, suggesting that the convertases from the classical and alternative pathways are likely to share their overall architecture and mode of substrate recognition. We propose an overall molecular model for the classical pathway C5 convertase in complex with C5, suggesting that C3b increases the affinity for the substrate by inducing conformational changes in C4b rather than a direct interaction with C5. C4b-specific features revealed by our structural studies are probably involved in the assembly of the classical pathway C3/C5 convertases and C4b binding to regulators. *The Journal of Immunology*, 2015, 194: 5488–5496.

The lectin pathway (LP) and the classical pathway (CP) (Fig. 1A) are two of the three main activation pathways within the complement system that are involved in resolution of infections, clearance of immune complexes, removal of apoptotic/necrotic cells, and stimulation of adaptive immunity (1). Both pathways are initiated by the binding of pattern recognition molecules (PRMs) to molecular patterns presented by pathogens

or altered self-surfaces. In the CP, the PRM C1q recognizes IgG or IgM present in immune complexes or bound to nonself surfaces, pentraxins, and other ligands (2). Activation of the LP is based on five PRMs—mannan-binding lectin, H/M/L-ficolin, and CL-L1/K1—that bind specific carbohydrate structures or acetylated molecules presented by pathogens (3). The PRMs in both pathways form complexes with paralogous serine proteases; C1q binds the heterotetramer C1r₂C1s₂, and the LP PRMs bind mannan-binding lectin-associated serine protease (MASP)-1 and MASP-2. Upon pattern recognition, the associated proteases become activated, and C1s or MASP-2 cleave C4 into C4b (195 kDa) and C4a (9 kDa). Although the small fragment has no established biological function, C4b acts as an opsonin and attaches to surface nucleophiles on the activator through their reaction with the thioester (TE) exposed upon C4 cleavage (4). The zymogen C2 may then bind C4b to form the CP proconvertase C4b2 (standardized notation for the C4b–C2 complex and other complexes is used throughout), in which C2 is cleaved by C1s, MASP-2, or MASP-1, and the C2b fragment is released. The C4b2a complex (the CP C3 convertase) remains on the activator and mediates downstream activation by cleaving C3 into C3b and C3a (5). Strong amplification of C3 cleavage proceeds through the alternative pathway (AP) via formation of the AP C3 convertase C3bBb. At a high density of C3b on the activator surface, C3b may combine with the C3 convertases, resulting in the CP and AP C5 convertases, C4b2a3b and C3bBb3b, respectively (6). In both the C3 and the C5 CP convertase, C4b acts as the noncatalytic substrate-binding subunit that presents the catalytic subunit C2a to the substrate. In the CP C5 convertase, C4b also contacts C3b, and they can even become covalently linked because C4b may offer a nucleophile for the cleavage of the TE in nascent C3b (7).

C4 is paralogous to complement proteins C3 and C5 and shares up to 30% sequence identity with the two proteins. However, maturation of C4 is more complex compared with C3 and C5 and includes generation of the three chains (α , β , and γ) from the precursor and the introduction of posttranslational modifications, including four *N*- and one *O*-linked glycosylations and sulfation of three tyrosine

*Department of Molecular Biology and Genetics, Aarhus University, DK-8000 Aarhus, Denmark; [†]Department of Biomedicine, Aarhus University, DK-8000 Aarhus, Denmark; and [‡]3rd Department of Internal Medicine, Semmelweis University, Budapest 1125, Hungary

ORCID: 0000-0001-6292-3319 (G.R.A.).

Received for publication January 13, 2015. Accepted for publication March 22, 2015.

G.R.A. was supported by Alexion Pharmaceuticals, The Lundbeck Foundation Nano-medicine Centre for Individualized Management of Tissue Damage and Regeneration, and the Novo-Nordisk Foundation through a Hallas-Møller Fellowship. S.M. received a Boehringer-Ingelheim Fonds Ph.D. fellowship.

S.M. conducted all steps of C4b preparation, crystal structure determination, and small angle x-ray scattering data analysis, assisted by G.R.A., Á.S., and Z.P. prepared the C4A-containing plasma. R.T.K. purified C4A and conducted the mass spectrometry analysis with assistance from S.V.P. G.R.A. designed the research and analyzed the data and results. S.M., S.V.P., Á.S., and G.R.A. wrote the manuscript. All authors read, corrected, and approved the final manuscript.

Coordinates and structure factors for the C4b crystal structure were deposited in the RCSB Protein Data Bank under accession code 4XAM.

Address correspondence and reprint requests to Prof. Gregers R. Andersen, Department of Molecular Biology and Genetics, Aarhus University, Gustav Wieds Vej 10C, DK-8000 Aarhus, Denmark. E-mail address: gra@mbg.au.dk

The online version of this article contains supplemental material.

Abbreviations used in this article: AP, alternative pathway; Asn-C, asparaginyl endopeptidase; C4BP, C4b binding protein; CCP, complement control protein; CP, classical pathway; CR, complement receptor; α 'CT, C-terminal region of the α '-chain; CUB, complement C1r/C1s, Uegf, Bmp1; CVF, cobra venom factor; DAF, decay acceleration factor; ESRF, European Synchrotron Radiation Facility; FH, factor H; FI, factor I; LP, lectin pathway; MASP, mannan-binding lectin-associated serine protease; MCP, membrane cofactor protein; MG, macroglobulin; MS, mass spectrometry; α 'NT, N-terminal region of the α '-chain; PDB, Protein Data Bank; PRM, pattern recognition molecule; RB, rigid body; SAXS, small angle x-ray scattering; TE, thioester; TFA, trifluoroacetic acid.

Copyright © 2015 by The American Association of Immunologists, Inc. 0022-1767/15/\$25.00

residues (8, 9) (Fig. 1B). C4 exists in two isotypes: the products of the two genes *C4A* and *C4B*. Although *C4A* and *C4B* differ in only 4-aa residues (*C4A*: P₁₁₂₀PCPVLD₁₁₂₅; *C4B*: L₁₁₂₀LSPVIH₁₁₂₅), they display markedly different hemolytic activities and affinities toward diverse substrates. Thus, *C4A* is more prone to attach to amine groups of an activator, whereas *C4B* reacts preferentially with hydroxyl groups (10, 11). Additionally, DNA and protein sequencing detected 23 polymorphic amino acid residues in both *C4A* and *C4B* (12).

Upon activation of C4, nascent C4b is expected to undergo conformational changes similar to those observed for C3/C3b, and the role of C4b in the CP convertases is assumed to be analogous to that of C3b in the AP convertases with respect to binding of the C3 and C5 substrates (13). There have been several structural studies of the AP C3 proconvertase and convertase (14–16), but it remains to be shown whether C4b2 and C4b2a are organized in the same manner or have additional unique features. There are also important differences between C3b and C4b with regard to their regulation on host cells and recognition by complement receptors (CRs). For example, an important regulator of C4b is C4b binding protein (C4BP), which acts as a cofactor for factor I (FI) cleavage of C4b into C4c and C4d via generation of an intermediate product iC4b (17–19); the main cofactor for C3b degradation, factor H (FH), is not considered a regulator of C4b. Another striking example is recognition of C3b/C4b and their degradation products by the CRs; only CR1 has an established function as a receptor for C4b (20), whereas there are five known receptors for C3b and its fragments (1). Hence, although C3b and C4b provide the same platform for substrates within the convertases, they are also highly distinct molecules that share only some of their binding partners.

To provide the structural basis for the dissection of the multiple functions of C4b, we determined the crystal structure of C4b at 4.2 Å resolution and characterized its solution structure by small angle x-ray scattering (SAXS).

Materials and Methods

Generation and crystallization of C4b

Human C4 was purified from outdated plasma pools without any attempt to separate isotypes C4A and C4B, essentially as described (21), although an additional step of anion-exchange chromatography on a Mono Q column (GE Healthcare) was added. To generate C4b, 50 mM Tris-HCl (pH 8.5), 30 mM glycine, 10 mM iodoacetamide, and 0.1% (w/w to C4) C1s (Complement Technology) were added to the purified C4. The reaction was incubated at 37°C overnight, and 1% (w/w to C4) C1 Esterase Inhibitor (Complement Technology) was added to the reaction mixture. The digest was subsequently loaded onto a 9-ml Source 15Q column (GE Healthcare) equilibrated in 20 mM HEPES-NaOH (pH 7.5), 200 mM NaCl and eluted with an 80-ml 200–600-mM NaCl gradient. Fractions containing C4b were pooled and dialyzed against 20 mM HEPES-NaOH (pH 7.5), 100 mM NaCl overnight. For deglycosylation, C4b was made 50 mM in Tris-HCl (pH 7) and 10% each (w/w to C4b) in GST-tagged EndoF1 and PNGase F. The reaction mixture was incubated at 30°C for 36 h, after which the endoglycosidases were removed by affinity chromatography on a GSTrap FF column (GE Healthcare). The flow-through containing deglycosylated C4b was dialyzed against 20 mM HEPES-NaOH (pH 7.5), 100 mM NaCl overnight and used for crystallization. Crystals of C4b were grown at 19°C in sitting drops made by mixing, in a 1:1:0.5 ratio, C4b at 4–5 mg/ml, reservoir solution containing 7.5% (w/v) PEG8000, 0.4 M MgCl₂, and 0.1 M Tris-HCl (pH 7), and a crystal seed stock solution. Crystals were cryoprotected by soaking them sequentially for 5–10 s in reservoir solution supplemented with 10, 20, and 30% (v/v) PEG400 prior to flash cooling in liquid nitrogen.

Data collection and structure determination

Data were collected at the European Synchrotron Radiation Facility (ESRF) (Grenoble, France) and processed with XDS (22). The structure was determined with molecular replacement using Phaser (23) and two search models based on macroglobulin (MG) domains 1–8 of C4 (RCSB Protein Data Bank [PDB] entry 4FXK) superimposed on the equivalent domains of C3b (RCSB PDB entry 2XWJ) and the TE domain derived from the structure of C4dg (RCSB PDB entry 1HZF). Models were iteratively

refined in Phenix.refine (24) and manually rebuilt in the O software (25). Atom positions were refined with simulated annealing and minimization, whereas temperature factors were refined with grouped B-factors and translation, libration, and screw-rotation groups. The two molecules in the asymmetric unit were restrained to each other with tight positional and loose B-factor noncrystallographic symmetry restraints. Electron-density maps used for model building were improved by real-space averaging. Figures were prepared with PyMOL v1.7.2.1 (<http://www.pymol.org>). Coordinates and structure factors for the C4b crystal structure were deposited in the RCSB PDB (<http://www.rcsb.org>) under accession code 4XAM.

SAXS data collection and modeling

C4b not treated with endoglycosidases was used for SAXS experiments after buffer exchange into 20 mM HEPES-NaOH (pH 7.5), 100 mM NaCl, 2 mM MgCl₂. Data were collected at the EMBL P12 beamline at PETRA III using a PILATUS 2M pixel detector. Scattering of the C4b samples at concentrations of 10, 5, and 2.5 mg/ml was recorded doing 20 exposures of 0.045 s with periods of 0.05 s for each sample in a temperature-controlled cell at 10°C with a path length of 1.5 mm. The sample-to-detector distance was 3.1 m, covering a range of momentum transfer $0.0028 < s < 0.45 \text{ \AA}^{-1}$ ($s = 4\pi\sin\theta/\lambda$). Normalization, radial averaging, buffer subtraction, and concentration correction of the data were done at the beamline by the automated pipeline (26). Radius of gyration, scattering at zero angle (I(0)) were calculated for each dataset using the ATSAS package (27) and compared. The two datasets collected at the highest protein concentrations (10 and 5 mg/ml) were merged using ALMERGE (26). Data analysis and rigid body (RB) refinement were done with ATSAS, using the data range $0 < s < 2.5 \text{ nm}^{-1}$. Calculation of theoretical scattering profiles of atomic structures and their fits to the experimental data were done with CRY SOL (28). Plots were prepared with GraphPad Prism 5.03. The input model for CORAL RB refinement was generated from the C4b crystal structure by addition of full biantenna Asn-linked glycan derived from RCSB PDB entry 3RY6.

Isolation of O-linked glycosylated peptides

To isolate the C4A isoform, we obtained plasma from a healthy donor (54 y old, female) with zero *C4B* gene copy number, as previously identified (29). C4A was purified essentially as C4 from normal plasma but on smaller columns. The conversion of C4A into C4Ac and C4Ad was performed through incubation of C4A overnight at 37°C in 50 mM Tris-HCl (pH 8.7), 30 mM glycine, 10 mM iodoacetamide with C1s (1:500 w/w to C4), FI (1:100 w/w to C4), and in-house purified C4BP (1:60 w/w to C4). The digest was separated by cation-exchange chromatography on a Source 15S column (GE Healthcare) equilibrated in 50 mM Tris-HCl (pH 7.6), 70 mM NaCl (buffer A). C4Ac and C4Ad were eluted with a linear gradient from 70 to 400 mM NaCl in buffer A. Fractions containing C4Ad were pooled and dialyzed into 50 mM NH₄HCO₃, 30 mM NaCl. To enable the analysis of O-linked glycosylation, the purified C4Ad was incubated overnight at 37°C with 1:30 (w/w to C4Ad) porcine trypsin (Promega) and subjected to sub-digestion using asparaginyl endopeptidase (Asn-C; R&D Systems) to obtain smaller peptides compatible with mass spectrometry (MS) analysis. Prior to digestion, Asn-C was activated by incubation in 50 mM sodium acetate (pH 4), 100 mM NaCl for 2 h at 37°C. Tryptic peptides were lyophilized and resuspended in 100 mM citric acid (pH 5.5), 100 mM NaCl, 5 mM DTT; activated Asn-C was added at an approximate ratio of 1:40 (w/w to C4Ad), and the solution was allowed to incubate for 16 h at 37°C. The digest was acidified by the addition of trifluoroacetic acid (TFA), and peptides were recovered using a StageTip (Thermo Scientific) containing C18 reverse-phase material. The peptides were eluted using 90% (v/v) acetonitrile, 0.1% (v/v) TFA, lyophilized, resuspended in 100 mM Tris-HCl (pH 7.4), 500 mM NaCl, and applied to a 5- μ l Jacalin/Agarose (InvivoGen) micro-column equilibrated in the same buffer. The column was washed with 100 mM Tris-HCl (pH 7.4), 500 mM NaCl, and peptides subsequently were eluted by the same buffer containing 20 mM α -methylgalactopyranoside. The eluate was acidified, and peptides were recovered on a C18 StageTip and eluted with a matrix solution of 2% (w/v) α -cyano-4-hydroxycinnamic acid, 70% (v/v) acetonitrile, 0.1% (v/v) TFA directly on the target plate for MALDI-MS analysis. The MS analysis was performed using an autoflex III Smartbeam instrument operated in reflector or linear mode and calibrated in the mass range of 1000–3200 Da using Peptide Calibration Standard (both from Bruker Daltonics).

Characterization of cysteine 1121

Purified C4Ad was incubated overnight at 37°C with porcine trypsin (1:30 w/w to C4Ad). The digest was subsequently acidified by the addition of TFA, and peptides were separated by ultra performance liquid chromatography reverse-phase chromatography using a BEH300 C18 column (2.1 mm \times 15 cm;

1.7 μm) operated by an ACQUITY UPLC System (Waters). The column was developed at a flow rate of 300 $\mu\text{l}/\text{min}$ using a 1% B/min linear gradient of solvent B (90% v/v acetonitrile, 0.08% v/v TFA) in solvent A (0.1% v/v TFA). Fractions were analyzed by MS using α -cyano-4-hydroxycinnamic acid. The fraction containing the C4A isotype peptide (L1100-R1126) was analyzed in both MS and tandem MS mode to validate the detected cysteinylolation of C1121. The lyophilized fraction was resuspended in 50 mM ammonium bicarbonate and 20 mM DTT and incubated at 37°C for 20 min. After that, the sample was made 40 mM in iodoacetamide and incubated at room temperature for 20 min to allow for derivatization of free thiol groups. The sample was acidified, and peptide was recovered with a StageTip containing C18 reverse-phase material and eluted directly onto the target plate using α -cyano-4-hydroxycinnamic acid, as described above.

Results

The architecture of C4b

We prepared crystallizable C4b of human complement component C4 by cleaving purified C4 with C1s and trimming the N-linked glycans with the endoglycosidases Endo F1 and PNGase F. The resulting C4b formed fragile crystals with a typical size of $50 \times 30 \times 5 \mu\text{m}$; after optimization of cryobuffers and mounting protocols, we obtained a complete data set extending to 4.2 Å resolution (Fig. 1C, Table I). The final model contained 1571 of 1637 C4b residues, whereas untraceable regions encompassed residues 1231–1255 (prenumbering of C4) in the TE domain, the C-terminal end of the C4b α' -chain (residues 1414–1428), and the beginning of the γ -chain (residues 1454–1463). The final C4b model has $R_{\text{work}}/R_{\text{free}}$ values of 0.217/0.273 (Table I), which is quite favorable considering the low resolution and the high R_{meas} of the diffraction data. C4b is organized into 12 domains, as previously described for C4 (21) (Fig. 1D). The six MG domains (MG1–6) and the linker region extensively interact with each other and form the core of the molecule. This represents the so-called “ β -ring,” because it comprises the entire β -chain; only the C-terminal region of the MG6 domain is located in the α' -chain. The MG7 and MG8 domains are situated on

the top edge of the β -ring and form contacts with the MG2, MG3, and MG6 domains. The complement C1r/C1s, Uegf, Bmp1 (CUB) and TE domains are located on the long edge of the β -ring and interact with MG2 and MG1, respectively (Fig. 1D). The TE, MG1, MG4, and MG5 domains constitute the bottom of the molecule. The C-terminal C345c domain is positioned at the opposite end of the molecule, on top of the MG7–8 domains, and connected to the MG7 domain through a disulfide bridge. The two noncrystallographic symmetry-related C4b molecules in our crystals vary in the orientation of the C345c domain by a 5-Å translation and a 12° rotation, with no other noteworthy differences between the two molecules.

The structural consequences of C4 cleavage

Our structure reveals the dramatic changes occurring upon release of C4a and the subsequent conformational transition of nascent C4b (Fig. 2, Supplemental Video 1). Overall, they are very similar to the conformational changes occurring upon activation of C3 (see below). Compared with C4, the major alterations in C4b are in the positions and orientations of the MG8, CUB, and TE domains. In C4, the TE is buried at the interface between the TE and MG8 domains (Fig. 2A); however, in C4b, it is highly exposed to nucleophiles from either solvent or an activator that may cleave the TE and form a covalent bond with Gln1013 (Fig. 2B). The location of the TE glutamine suggests that the C4b molecule attaches to activator surfaces with its bottom (the MG1, MG4, MG5, and TE domains) located closest to the activator, whereas the C345c domain points away from the activator (Fig. 2B).

In C4, the MG8 and MG3 domains are held in position by the anaphylatoxin domain; upon its release as C4a, the MG8 domain rotates by 53° and translates by 29 Å (Fig. 2, Supplemental Video 1). The MG3 domain also rotates by 18° and establishes hydrophobic interactions with the relocated MG8 domain in C4b. The

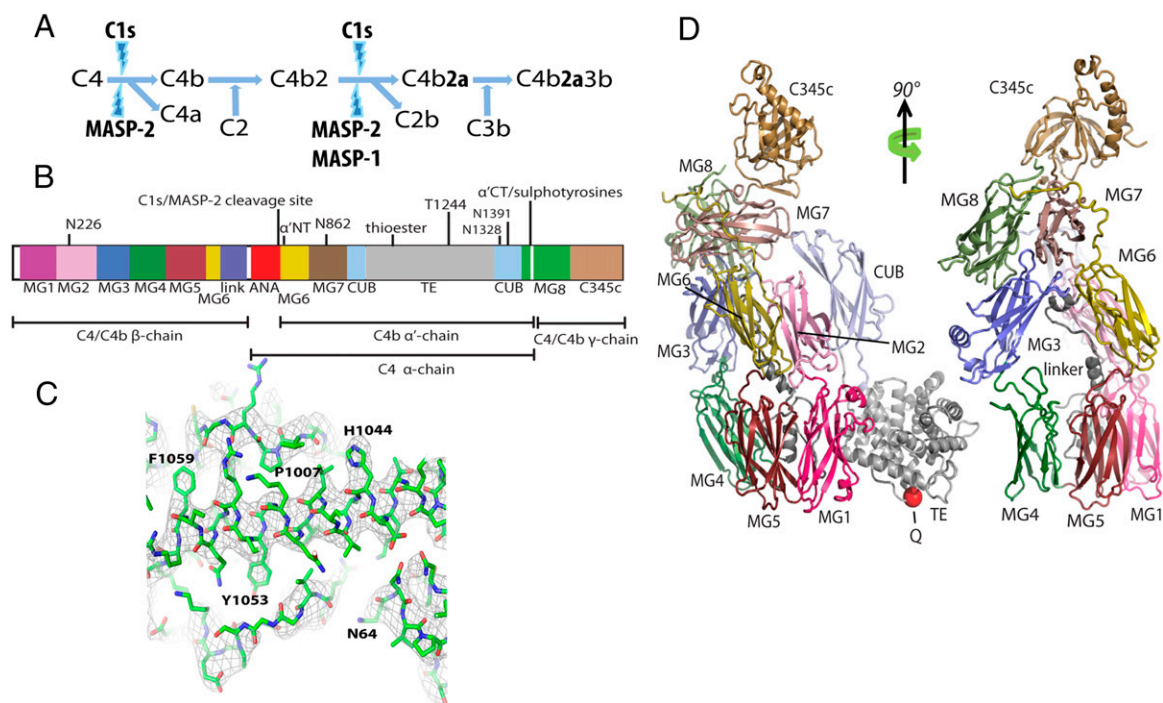


FIGURE 1. The function of C4 in complement and the structure of C4b. (A) Proteolytic processing and function of C4 and C4b in the CP (involving C1s) and the LP (involving MASP-1 and MASP-2). Active proteases are in bold font. C4b2a and C4b2a3b are the C3 and C5 convertases, respectively. (B) Schematic representation of the chain and domain structure of C4 and C4b. Four N-linked (N226, N862, N1328, N1391) and one O-linked (T1244) glycosylation sites are labeled. (C) The final model of C4b together with an omit 2mF_o-DF_c electron density map contoured at 1 σ calculated following simulated annealing of a model with residues P1039-F1059 from the TE domain omitted. (D) The structure of C4b in two orientations. The position of the TE glutamine residue is indicated by the red sphere marked “Q.” The domains are colored as (B).

Table I. Statistics for data collection and model refinement

Data Collection and Processing	
Beam line/ λ (Å)	ESRF ID23-1/0.9840
Space group	P2 ₁
Unit cell parameters	
a, b, c (Å)	121.50, 161.08, 131.60, 107.262
β (°)	
Resolution (Å)	49.54–4.20 (4.39–4.20)
R_{meas} (%)	28.5 (83.4)
$I/\sigma I$	7.15 (2.56)
Completeness (%)	98.3 (99.3)
Redundancy	7.04 (7.15)
Refinement	
Resolution (Å)	49.54–4.20 (4.39–4.20)
No. reflections	34,849
$R_{\text{work}}/R_{\text{free}}$ (%)	21.7/27.3 (30.3/39.4)
No. protein atoms	24,258
RMS deviations from ideality	
Bond lengths (Å)/angles (°)	0.010/1.43
Average B values (Å ²)	127.7
Ramachandran plot ^a (%)	
Favored/allowed/outliers	91.65/8.07/0.29

The values in parentheses are for outer resolution shell. $R_{\text{meas}} = \left(\sum_{hkl} \sqrt{(n/(n-1)) \sum_{j=1}^n |I_{hklj} - \langle I_{hkl} \rangle|} \right) / \sum_{hkl} \sum_j I_{hklj}$ for the intensity of reflection hkl measured n times.

R -factor = $\left(\sum_n ||F_o| - k|F_c|/ \sum_n |F_o| \right)$, where F_o and F_c are the observed and calculated structure factor, respectively, and k is a scaling factor. R_{free} -factor is identical to the R -factor on a subset of test reflections not used in refinement.

^aValues given by MolProbity.

RMS, root mean square.

displacement of MG8 disrupts its contacts with the TE and CUB domains, allowing these to rotate by 112 and 55° and move by 59 and 42 Å, respectively, toward the MG1 and MG2 domains along the long side of the β -ring core (Fig. 2, Supplemental Video 1). As a consequence, the MG7 domain, which is connected to the CUB domain, rotates by 35°, relocates to form the “ceiling” of the MG2 and MG6 domains, and engages in new interactions with the MG8 domain (Figs. 1D, 2B). The MG7 domain has another important function in C4b: it holds the newly generated N-terminal region of

the α' -chain (α' NT), consisting of residues 757–780. This region encompasses several acidic residues (E763, E764, D768, E769, E770, E771) believed to participate in the interaction of C4b with C2 (30). To reach this location, the α' NT region has to move out through a narrow opening formed between the MG2, MG3, and MG6 domains and the linker region (Fig. 2, Supplemental Video 1). Finally, the C345c domain is translated by 10 Å and rotated by 42° as a result of the loss of its contacts with the CUB domain. However, the location of this domain is likely variable, as indicated by our SAXS studies (see below). In summary, release of C4a induces dramatic conformational changes in C4b that position the TE domain in the vicinity of the MG1 domain and expose the TE to nucleophiles. The MG1–6 domains form a stable structural unit supporting the movements of the MG7, MG8, CUB, and TE domains.

The solution structure of C4b

Crystallization of proteins can induce conformational artifacts by crystal packing. Furthermore, because C4b could only be crystallized upon trimming of the Asn-linked glycans, we decided to investigate the solution conformation of C4b with glycans by performing SAXS experiments (Supplemental Fig. 1). During RB refinement with CORAL, four RBs were defined within C4b corresponding to all MG domains, as well as the CUB, the TE, and the C345c domains (Fig. 3A). With all RBs locked in the positions as in the C4b crystal structure and modeling of residues not modeled in the crystal structure, a mean $\chi^2 = 2.99$ of the fit of the model to the experimental SAXS data was observed. With four glycans added as separate RBs, the mean χ^2 decreased to 2.12, justifying their addition. By allowing the CUB and C345c domains to move, mean χ^2 further decreased to 1.82, and the additional release of the TE domain gave a χ^2 value of 1.40. In the C4b crystal structure, a contact between the MG1 and TE domains was observed; however, in the CORAL models obtained with the above scenario, the TE domain separated from the MG1 domain. To explore this difference between the crystal and solution structures, we evaluated three restraints based on the MG1–TE domains contact with lengths of 6, 10, and 14 Å, which gave rise to mean χ^2 values of 1.73, 1.51, and 1.43, respectively. This suggested that the contact observed in the

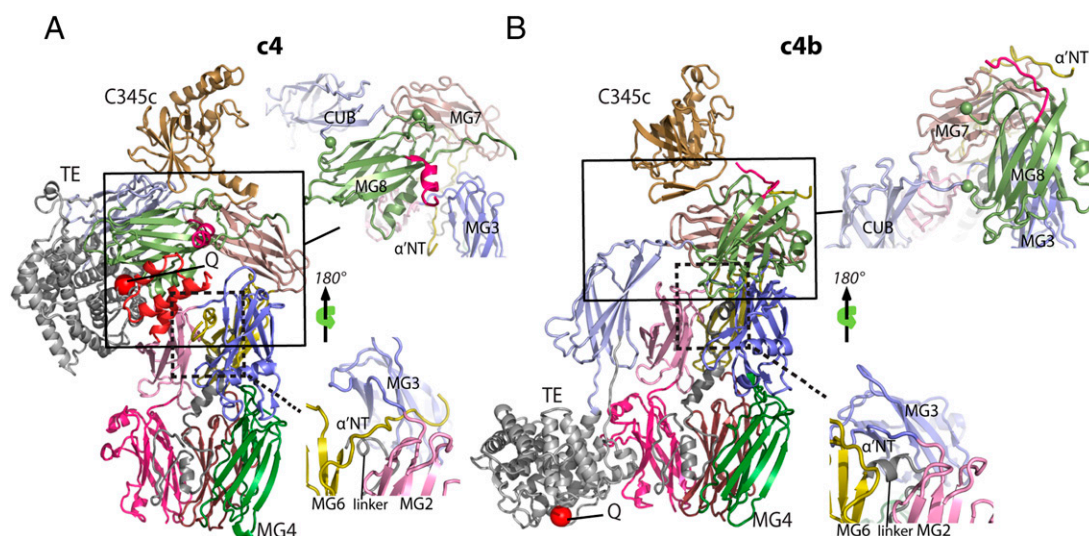


FIGURE 2. The structural changes accompanying activation of C4 and its transition to C4b. Overall views of C4 (RCSB PDB entry 4FXK) (A) and C4b (B) with close-up views of the two regions, the MG8 domain (close-up view, solid box) and the α' NT (close-up view, dashed box) in the two states. The two close-up views are related by a 180° rotation, because the domains shown in these views are located on opposite faces of C4 and C4b. The MG8 domain undergoes a large rotation and translation upon release of C4a. The α' NT is inserted between the MG2, MG3, and the linker region in C4, whereas it has moved out through the hole formed by these domains in C4b and now extends toward the MG7 domain. The C4 and C4b structures are superimposed on the MG1–6 domains and shown separately. Green spheres mark the beginning and end of the MG8 domain. The α' NT region is displayed in yellow, and the α' CT/sulfotyrosine region is displayed in magenta. The TE glutamine (“Q”) is shown as a red sphere.

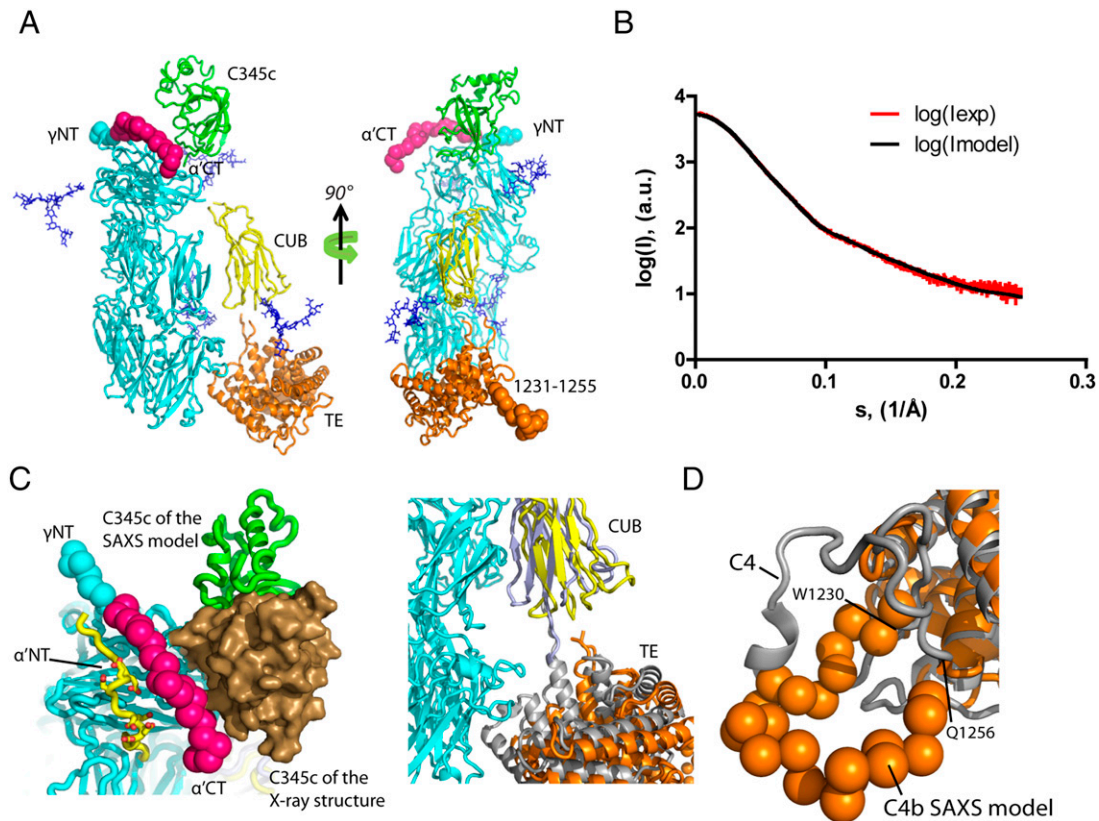


FIGURE 3. The SAXS model of C4b. The MG domains and the linker region are shown in cyan. *N*-linked glycans are displayed as blue sticks. Dummy atom regions obtained during CORAL refinement representing the regions missing in the crystal structure are shown as spheres. The α' CT region is displayed in magenta, the N-terminal end of the γ -chain (γ NT) is in cyan, and the 1231–1255 loop of the TE domain is orange. **(A)** Overview of the SAXS model of C4b, the coloring reflects the RBs used during CORAL refinement. **(B)** The CRYSOLOG fit of the theoretical scattering calculated for the SAXS model (Imodel) to the experimental scattering (I_{exp}) for the best model. **(C)** Differences in conformations of the C345c domain (*left panel*) and CUB–TE domains (*right panel*) between the crystal structure and SAXS model of C4b. The CUB, TE, and C345c domains of the C4b crystal structure are colored light blue, gray, and brown, respectively. Dummy atom modeling places the α' CT (magenta spheres) parallel to the α' NT, with its acidic residues displayed as sticks (*left panel*). **(D)** Dummy atom model of the 1231–1255 loop in the TE domain in comparison with the ordered loop (gray) from the C4 crystal structure.

crystalline state is stabilized by crystal packing, whereas in solution the two domains are separated slightly (Fig. 3C). As the final SAXS-derived model of C4b, we present the CORAL solutions derived from the scenario with the 14 Å MG1–TE contact restraint described above with the best $\chi^2 = 1.41$ (Fig. 3A, 3B).

The SAXS models indicate the structural organization of residues 1231–1255 within the TE domain that were not traceable in the C4b crystal structure, suggesting its flexibility, as already proposed by the structure of the C4b fragment C4dg (31). These residues protrude from the TE domain in a roughly U-shaped exposed loop in all SAXS models (Fig. 3A, 3D). In C4, this region is folded into an ordered loop stabilized by interaction with the C4 CUB domain. Another functionally important area in C4 is the α' CT/sulfotyrosine region encompassing residues 1405–1427. In C4, residues 1404–1415 form an α -helix that is followed by the three sulfated tyrosines (Y1417, Y1420, Y1422) of importance for C4 interaction with C1s and MASP-2 (21, 32). In contrast, residues 1404–1413 adopt a random coil conformation in C4b, whereas the residues 1414–1427 could not be traced. Our SAXS modeling suggests that, in solution, the α' CT region runs across the MG7 domain roughly parallel to the α' NT (Fig. 3C). In addition to the position of the TE domain, another major difference between the crystal structure and the SAXS model is the reorientation of the C345c domain by almost 90° (Fig. 3C). We tested the significance of this by repeating the restrained CORAL scenario described above where the C345c domain was fixed together with the MG domains as observed in the crystal structure, but this increased the average χ^2

from 1.41 to 1.52, justifying release of the C345c domain during refinement. In conclusion, our SAXS studies confirm the overall conformation of C4b observed in the crystalline state but also identified two significant deviations from the crystal conformation in solution. Furthermore, the SAXS modeling suggests the approximate location of functionally important and exposed regions that could not be modeled in the crystal structure because of flexibility.

Two posttranslational modifications in the C4 TE domain

Human C4A recovered from cerebrospinal fluid was identified to contain an *O*-linked core 1 glycan (Gal-GalNAc-Thr; T-Ag) at Thr¹²⁴⁴ (8), meaning that it is exposed in the loop 1231–1255 discussed above (Fig. 3D). To confirm these findings, we subjected the purified C4d fragment of C4A (C4Ad) to proteolytic cleavage using both trypsin and Asn-C. To enrich for *O*-linked glycopeptides, the generated peptides were fractionated by lectin-affinity chromatography using Jacalin/Agarose. Analysis of the isolated peptides identified peaks representing the A1240-R1248 peptide (m/z_{calc} 895.5) modified by Gal-GalNAc (365.3 Da; m/z_{obs} 1260.63) or by its sialylated variant (656.6 Da; m/z_{obs} 1551.52) (Supplemental Fig. 2A). To further validate that these ions indeed represented the A1240-R1248 peptide, we subjected m/z 1260.63 to MS/MS analysis (Supplemental Fig. 2B). This analysis generated fragment ions representing the peptide containing GalNAc only (m/z 1098.51) and the peptide with no carbohydrate moiety (m/z 895.39). Moreover, we could assign ions representing the y2 and y4 fragments of the unglycosylated peptide (Supplemental Fig. 2B). Our data cannot

conclusively distinguish between residues S1242 or T1244 as carrier of the *O*-linked glycan, but they are consistent with the finding by Halim et al. (8) identifying Thr1244 as the modified residue. Interestingly, this residue is almost strictly conserved, which points to a functional importance of the *O*-linked glycan.

Additionally, human C4A encompasses an isotypic cysteine residue at position 1121. Another isotypic residue of C4B, H1125, was suggested to form an acyl-imidazole intermediate with the TE glutamine upon C4B activation (33). This implies that a free thiol group at position 1121 in C4A could play a role in TE cleavage or formation of a de novo disulfide bridge with C1010 released from the TE in C4b. To evaluate the status of residue 1121, we separated tryptic peptides generated from C4Ad by reverse-phase chromatography and analyzed the resulting fractions by MALDI-MS. One fraction presented an ion of m/z 3194.89, corresponding to the peptide encompassing C1121 (m/z_{calc} 3076.35) modified by cysteinylated (119 Da; m/z_{calc} 3194.89) (Supplemental Fig. 2C, upper panel). To confirm this, we subjected the peptide to reduction and alkylation, producing the *S*-carbamidomethylated peptide represented by m/z 3132.91 (Supplemental Fig. 2C, lower panel). The position of the modifications was validated further by tandem MS analysis, showing that C1121 is cysteinylated in human C4A. This finding is consistent with previous studies showing that C4b generated by digestion of C4, which was isolated from pooled plasma and expected to contain almost equivalent amounts of C4A and C4B, has a maximum of one free thiol group/C4b molecule (34). Hence, human C4A does not contain a free thiol, and C1121 and C1010 are separated by 15 Å in C4b, further arguing that disulfide formation in nascent C4b is unlikely to occur (Supplemental Fig. 2D).

Structural mapping of the C4 isoforms and allotypes

C4 is the most heterogeneous protein of the complement system. In addition to the two isoforms of the *C4* gene, *C4A* and *C4B*, 23 allotypes of the genes were reported. With the C4 and C4b structures available, we can map these variants onto the two major functional states of C4 (Fig. 4). This shows that 14 of these variable residues are solvent accessible each in C4b and in C4 (additional variable residues are located in the C4a moiety). Eleven of the variants are located in the TE domain, and seven of them are exposed in C4b (Fig. 4). These variants are the basis for the serological distinction between the Rodgers or Chido blood group Ags (35). Our analysis suggests that eight of the variable isotypic and allotypic residues are close to the activator in C4b (Fig. 4). Hence, similar to the differential reactivity toward nucleophiles of the nascent TE in C4A and C4B, the variation within surface-exposed residues close to the activator might broaden the repertoire of interactions that can occur between C4b and activators.

Discussion

During the last decade, a wealth of structures of complement proteins has profoundly improved our understanding of structure–function relationships within the complement system. C3 and C4 are important proteins of the complement cascade, because their proteolytic fragments C3b and C4b act as opsonizing molecules, as well as the central subunits in the C3/C5 convertases providing a platform for bringing together the catalytic subunit and the substrate for proteolysis. Although several crystal and solution structures involving C3b are known, there has been a complete lack of structural information concerning C4b. The present study provides this information and identifies the structural principles shared by C3b and C4b, as well as several important C4b-specific features.

Structural similarity of C3b and C4b was expected, and comparison of our C4b structure with various structures containing C3b indeed reveals a remarkable resemblance of the two paralogues. The

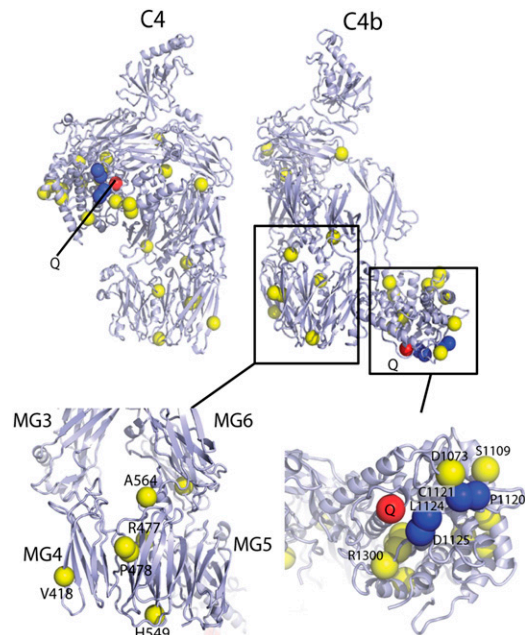


FIGURE 4. The position of allotypic (yellow spheres) and isotypic (blue spheres) residues mapped on the structure of C4b (upper right panel) and C4 (upper left panel). Close-up views of the MG4–6 (lower left panel) and the TE domain (lower right panel). The glutamine of the TE domain (Q) is shown as a red sphere. The conformational change exposes some allotypic residues and all the isotypic residues relatively close to the activator.

MG1–8 domains in C3b and C4b are arranged in a very similar manner (Fig. 5A), which is likely to be dictated by the function of the MG4, MG5, and MG7 domains in both C3b and C4b as interactors with the substrate within the convertases (13) and their common regulators (see below). Furthermore, the structural similarity extends to the location of the CUB and TE domains observed in our C4b crystal structure and all known C3b-containing crystal structures. In particular, the MG1–TE interaction is preserved between crystal structures of C3b and C4b. Likewise, the presentation of the α' NT region on the surface of the MG7 domain (Fig. 3C) is shared between C3b and C4b.

The close conformational match between C3b and C4b further strengthens the idea that the CP proconvertase C4b2 and convertase C4b2a are similar in structure to their AP equivalents C3bB and C3bBb and the fluid-phase convertase formed by cobra venom factor (CVF) and Bb, CVFBb (13). Within the AP proconvertase, the C3b α' NT region is sandwiched between the C3b MG7 domain and factor B (14), and the virtually identical presentation of the α' NT region in C4b on top of the MG7 domain suggests that this will apply to the CP proconvertase as well (Supplemental Fig. 3A). This is in accordance with reduced C2 binding to C4b carrying mutations in two acidic clusters within the α' NT region (30). Additionally, in our model of the CP proconvertase, the highly acidic and flexible α' CT/sulfotyrosine region has the potential to interact with nearby positively charged areas of C2 (Supplemental Fig. 3A, 3B).

Our C4b structure also provides a means for investigating the mysterious architecture of the CP C5 convertase C4b2a3b, in which the presence of C3b shifts the specificity from C3 to C5. The SAXS-based modeling of residues 1231–1255 in the TE domain of C4b shows that the loop is highly exposed to the solvent (Fig. 3D). This loop is known to be involved in the interaction of C4b with C3b within the CP C5 convertase (7). Therefore, the exposure of these residues and their accessibility for C3b might be necessary for establishing contacts between C4b and C3b. Additionally, the strictly conserved Ser1236 within the exposed loop can act as a nucleophile

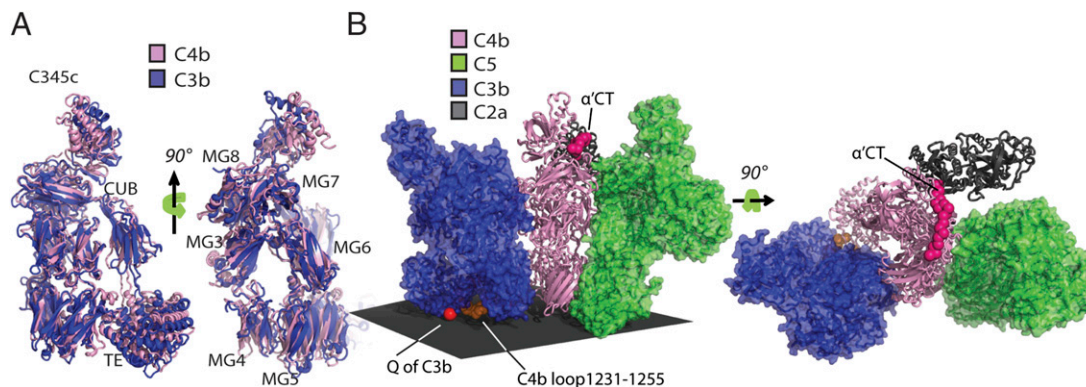


FIGURE 5. A highly conserved conformation of C3b/C4b and the model of the CP C5 convertase complex. **(A)** Comparison of the C3b (RCSB PDB entry 2I07) and C4b crystal structures demonstrates the striking similarities in their conformation. The structures were superimposed on the MG1–5 domains. **(B)** The model of the CP/LP C5 convertase in complex with C5 built based on combining the structures of C4b, the C3b–FH CCP1–4 complex (RCSB PDB entry 2WII), the C3b–FH CCP19–20 complex (RCSB PDB entry 4ONT), the C5–C3b complex (RCSB PDB entry 3PVM), the C3bBb complex (RCSB PDB entry 2WIN), and C2a (RCSB PDB entry 2ODP). The C3b molecule (in blue) was placed by positioning the glutamine (Q) of the C3b TE domain at the apex of the C4 loop and then rotating C3b such that its FH binding sites are facing C4b (see also Supplemental Fig. 3C, 3D). The proximity of the α' CT region to both C2a and C5 is shown (*right panel*).

attacking the TE in nascent C3b, leading to the formation of covalent C4b–C3b heterodimers (7). The SAXS structure of C4b hints at how C3b can be located in the CP C5 convertase because Ser1236 is the primary contact point between C4b and C3b in this convertase. By placing the cleaved TE of a C3b molecule roughly at the apex of the exposed C4b loop, we can search for possible arrangements of the C3b molecule relative to C4b (Supplemental Fig. 3D). We assume that C3b does not change dramatically in conformation when it is incorporated into the CP C5 convertase. This leads us to suggest a model for the CP C5 convertase in which the longest principal axes of C4b and C3b are arranged roughly in parallel (Fig. 4B, Supplemental Fig. 3D). In the model, we chose to position the C3b binding sites for FH complement control protein (CCP)1–4 and CCP19–20 (Supplemental Fig. 3C) toward C4b, suggesting that binding of these modules to C3b would interfere with a close approach of C3b and C4b in the CP C5 convertase, and additional steric hindrance may be exerted by the intervening CCP modules 5–18 of FH believed to be looping out between CCP4 and CCP19 (36, 37). The resulting model for the CP C5 convertase offers an explanation for prior biochemical data showing that FH, in contrast to factor B, inhibits lysis of erythrocytes (38) and that C3b covalently bound to C4b is protected from FH-dependent FI degradation (39). However, our model for the CP C5 convertase must be considered with caution, keeping in mind that conformation of the loop containing the C4b–C3b contact point (Ser1236) is modeled by the use of low-resolution SAXS data. If this loop adopts a radically different conformation in activator-bound C4b, the suggested parallel orientation of C3b and C4b in the CP C5 convertase may not be possible.

An important feature of our CP C5 convertase model is that the C3b molecule cannot obtain direct contact with C5 because of the proximity between the two TE domains of C3b and C4b, suggesting that C3b alters the substrate specificity from C3 to C5 solely by altering the conformation of the C4b2a complex. An overall putative model of the substrate-bound C5 convertase is displayed in Fig. 5B; the MG6 domain of C3b is close to the MG3 and MG8 domains of C4b. Because the latter two domains are adjacent to the substrate-binding C4b domains MG4 and MG7, respectively, it is conceivable that an allosteric effect leading to higher C5 affinity could be transmitted through C3b contacts with these C4b domains. Based on the ability of both anti-C4 and anti-C3 Abs to inhibit substrate binding by the CP C5 convertase, it was suggested previously that both C4b and C3b form direct contact with C5 (6).

However, our model is also consistent with these data: the anti-C3 Abs might simply interfere with the C3b–C4b interaction proposed in this article.

By combining our C4b and C5–C3b structures, we suggest that the C4b-binding area for the substrates C3 and C5 is within the domains MG4, MG5, and MG7. This suggestion is supported by studies showing that changes in the two variant residues in the MG5 domain of C4b, R477, and P478 (Fig. 4), to tryptophan and leucine, respectively, cause defects in C5 binding by the CP C5 convertase (40, 41), and alanine scanning of residues in their vicinity also results in mutant C4b molecules impaired in CP C5 convertase activity (42). Moreover, the α' CT is also located near C5 in our substrate-convertase model (Fig. 5B), which suggests that, as in the C4:MASP-2 complex, the α' CT region may bridge the substrate and the catalytic subunit. In summary, the structures of C3b and C4b are surprisingly similar. This allows us to combine structural studies of the AP convertases with biochemical and genetic data on the CP proteins and convertases. Thereby, we are able to propose overall working models for the CP convertases.

The C4b α' CT/sulfonyltyrosine region is an extremely acidic region harboring 11 negative charges within residues 1405–1427. We and other investigators provided data showing that it facilitates C1s/MASP-2 recognition of C4 (21, 43) by acting as electrostatic “Velcro” between the SP domain of the protease and the C4 anaphylatoxin domain. However, the observed changes within the α' CT region in C4b compared with C4 prompted us to speculate on other functions for this C4-specific region. Our SAXS modeling indicated that the α' CT region is associated with the MG7 domain and is located close to the C345c domain of C4b and the acidic α' NT region (Fig. 3C). Again, the low resolution of the SAXS data means that suggestions based on the resulting RB models must be treated with caution. Even if the conformation of the α' CT region is different from that proposed by SAXS, this highly negatively charged and flexible region has a length and flexibility that probably enable it to interact with C2, C2a, convertase substrates, and even regulators.

Our crystal and SAXS structures differ with respect to the location of the C345c, TE, and CUB domains, suggesting that C4b harbors some degree of flexibility, which may be a prerequisite for the function of the molecule. The flexibility of the C345c domain is a well-known phenomenon, because reorientation of this domain is also observed in structures involving C3b (14, 15, 44). In C4/C4b,

this flexibility is probably required for its multiple functions because it is both a carrier of C2/C2a protease in the (pro)convertases and a binding site for MASP-2 and C1s proteases during C4 cleavage (21). The ability of the TE domain to dissociate from the MG1 domain, as observed in the SAXS structure, may support C4b function as an opsonin by improving its chance for covalent attachment to the myriad of activator surfaces that it encounters. Very recent solution structures of C3b and C3(H₂O) in 137 mM NaCl indicated that the TE domain of C3b can separate by up to 60 Å from the MG1 domain, whereas a compact conformation resembling the C3b crystal conformation was observed in 50 mM NaCl (45). It was suggested that the low salt concentrations used for crystallization of C3b induced the compact conformation with the TE–MG1 contact. We observed the opposite trend; our SAXS modeling of C4b in solution indicates that the TE domain can move slightly away from the MG1 domain in the presence of 100 mM NaCl, whereas C4b exhibits the MG1–TE interaction inside crystals grown in the presence of 400 mM MgCl₂. Cofactor-assisted FI cleavage presumably requires a rather fixed conformation of C3b and C4b to dock C3b/C4b, the regulator, and FI simultaneously into a productive complex (46). Therefore, the crystal structures of C3b and C4b are likely to resemble a substrate conformation for cofactor-assisted FI degradation. This does not exclude that the TE and CUB domains may be more or less separated from the MG domains in other functional states of C3b and C4b.

Binding of FH CCP1–4 domains relies on interaction with the C3b α'NT region, the MG1, MG2, MG6, and MG7 domains, and the CUB and TE domains (46). Thereby, FH provides a platform for positioning FI correctly relative to the C3b CUB domain for subsequent cleavage, and this binding mode probably applies to membrane cofactor protein (MCP) and decay acceleration factor (DAF) as well (46). The cofactors themselves also have a conserved structure. Usually, three consecutive CCP domains are required for cofactor activity, and these three are linked in an almost linear structure (47), whereas a bend occurs between the third and the following CCP domains, which may not be required for cofactor activity. The high conservation between C3b and C4b, the conserved positions of FI cleavage sites in the CUB domains of C3b and C4b, and the conserved structure of the regulators led us to suggest a simplistic model for the interaction of C4b with its regulators (Supplemental Fig. 3E). This suggests that cofactors (C4BP, MCP, CR1, MCP, the vaccinia virus complement control protein VCP, and the rodent specific Crry) for FI degradation bind to C4b in a manner similar to that observed in the C3b–FH complex. In agreement with this proposal, C4c encompassing all of the MG domains and the α'NT region binds only three times weaker than does C4b to C4BP (48). In the proposed binding mode, the CCP1 and CCP2 domains of C4b regulators would align with the C4b α'NT region, like in the C3b–FH complex, and significantly contribute to binding of the whole regulator molecule to C4b. In addition to the α'NT, the nearby highly acidic α'CT/sulfotyrosine region of C4b might play a role by interacting with basic residues in a regulator's CCP1–CCP2 domains (Supplemental Fig. 3D). All C4b cofactors indeed have several lysines and arginines that would face the α'CT and α'NT regions in a C3b–FH–like binding mode. The importance of a cluster of basic residues exactly in the C4BP CCP1–CCP2 domains for cofactor activity against C4b, as well as the strong electrostatic nature of the intermolecular interaction C4b–C4BP, were shown earlier by mutagenesis and binding studies (49). Another regulator of C4b, DAF, likewise contains positively charged residues in its CCP2 domain and the linker between CCP2 and CCP3 that might interact with the two aforementioned acidic C4b regions.

In conclusion, determination of both the crystal and solution structures of C4b confirms the anticipated unifying structural prin-

ciples for C3b and C4b, supporting their shared functions as opsonins and as platforms for binding the catalytic subunit and substrates in convertases. Additionally, our results highlight the flexibility of the TE domain loop 1231–1255 and the sulfotyrosine-containing α'CT region specific to C4 and suggest important functions of these elements within the CP convertases. Our study sets the scene for dissecting structural requirements of C4b binding of C2/C2a, the role of C3b in shifting the specificity of the CP C3 convertase to C5, and the recognition of C4b by DAF and the FI cofactors CR1, C4BP, Crry, and MCP.

Acknowledgments

We thank F.X. Gomis-Ruth for endoglycosidase expression vectors, the beam-line staffs at PETRA III and ESRF for support during data collection, and Jan Skov Pedersen for help with SAXS data processing and RB refinement.

Disclosures

The authors have no financial conflicts of interest.

References

- Ricklin, D., G. Hajishengallis, K. Yang, and J. D. Lambris. 2010. Complement: a key system for immune surveillance and homeostasis. *Nat. Immunol.* 11: 785–797.
- Kojouharova, M., K. Reid, and M. Gadjeva. 2010. New insights into the molecular mechanisms of classical complement activation. *Mol. Immunol.* 47: 2154–2160.
- Kjaer, T. R., S. Thiel, and G. R. Andersen. 2013. Toward a structure-based comprehension of the lectin pathway of complement. *Mol. Immunol.* 56: 222–231.
- Law, S. K. 1983. The covalent binding reaction of C3 and C4. *Ann. N. Y. Acad. Sci.* 421: 246–258.
- Kerr, M. A. 1980. The human complement system: assembly of the classical pathway C3 convertase. *Biochem. J.* 189: 173–181.
- Takata, Y., T. Kinoshita, H. Kozono, J. Takeda, E. Tanaka, K. Hong, and K. Inoue. 1987. Covalent association of C3b with C4b within C5 convertase of the classical complement pathway. *J. Exp. Med.* 165: 1494–1507.
- Kim, Y. U., M. C. Carroll, D. E. Isenman, M. Nonaka, P. Pramoonjago, J. Takeda, K. Inoue, and T. Kinoshita. 1992. Covalent binding of C3b to C4b within the classical complement pathway C5 convertase. Determination of amino acid residues involved in ester linkage formation. *J. Biol. Chem.* 267: 4171–4176.
- Halim, A., U. Rüetschi, G. Larson, and J. Nilsson. 2013. LC-MS/MS characterization of O-glycosylation sites and glycan structures of human cerebrospinal fluid glycoproteins. *J. Proteome Res.* 12: 573–584.
- Hortin, G., H. Sims, and A. W. Strauss. 1986. Identification of the site of sulfation of the fourth component of human complement. *J. Biol. Chem.* 261: 1786–1793.
- Law, S. K., A. W. Dodds, and R. R. Porter. 1984. A comparison of the properties of two classes, C4A and C4B, of the human complement component C4. *EMBO J.* 3: 1819–1823.
- Isenman, D. E., and J. R. Young. 1984. The molecular basis for the difference in immune hemolysis activity of the Chido and Rodgers isotypes of human complement component C4. *J. Immunol.* 132: 3019–3027.
- Blanchong, C. A., E. K. Chung, K. L. Rupert, Y. Yang, Z. Yang, B. Zhou, J. M. Moulds, and C. Y. Yu. 2001. Genetic, structural and functional diversities of human complement components C4A and C4B and their mouse homologues, Slp and C4. *Int. Immunopharmacol.* 1: 365–392.
- Laursen, N. S., K. R. Andersen, I. Braren, E. Spillner, L. Sottrup-Jensen, and G. R. Andersen. 2011. Substrate recognition by complement convertases revealed in the C5-cobra venom factor complex. *EMBO J.* 30: 606–616.
- Fornieris, F., D. Ricklin, J. Wu, A. Tzekou, R. S. Wallace, J. D. Lambris, and P. Gros. 2010. Structures of C3b in complex with factors B and D give insight into complement convertase formation. *Science* 330: 1816–1820.
- Rooijackers, S. H., J. Wu, M. Ruyken, R. van Domselaar, K. L. Planken, A. Tzekou, D. Ricklin, J. D. Lambris, B. J. Janssen, J. A. van Strijp, and P. Gros. 2009. Structural and functional implications of the alternative complement pathway C3 convertase stabilized by a staphylococcal inhibitor. *Nat. Immunol.* 10: 721–727.
- Torreira, E., A. Tortajada, T. Montes, S. Rodríguez de Córdoba, and O. Llorca. 2009. 3D structure of the C3bB complex provides insights into the activation and regulation of the complement alternative pathway convertase. *Proc. Natl. Acad. Sci. USA* 106: 882–887.
- Blom, A. M., B. O. Villoutreix, and B. Dahlbäck. 2004. Complement inhibitor C4b-binding protein—friend or foe in the innate immune system? *Mol. Immunol.* 40: 1333–1346.
- von Zabern, I., and I. Gigli. 1982. Conformational changes in complement component C4 induced by activation, treatment with amines, chaotropes, or freezing-thawing, detectable by radioiodination using lactoperoxidase. *J. Immunol.* 128: 1439–1442.
- Nagasawa, S., C. Ichihara, and R. M. Stroud. 1980. Cleavage of C4b by C3b inactivator: production of a nicked form of C4b, C4b', as an intermediate cleavage product of C4b by C3b inactivator. *J. Immunol.* 125: 578–582.

20. Krych-Goldberg, M., and J. P. Atkinson. 2001. Structure-function relationships of complement receptor type 1. *Immunol. Rev.* 180: 112–122.
21. Kidmose, R. T., N. S. Laursen, J. Dobó, T. R. Kjaer, S. Sirotkina, L. Yatime, L. Sottrup-Jensen, S. Thiel, P. Gál, and G. R. Andersen. 2012. Structural basis for activation of the complement system by component C4 cleavage. *Proc. Natl. Acad. Sci. USA* 109: 15425–15430.
22. Kabsch, W. 2010. Integration, scaling, space-group assignment and post-refinement. *Acta Crystallogr. D Biol. Crystallogr.* 66: 133–144.
23. McCoy, A. J., R. W. Grosse-Kunstleve, P. D. Adams, M. D. Winn, L. C. Storoni, and R. J. Read. 2007. Phaser crystallographic software. *J. Appl. Cryst.* 40: 658–674.
24. Afonine, P. V., R. W. Grosse-Kunstleve, N. Echols, J. J. Headd, N. W. Moriarty, M. Mustyakimov, T. C. Terwilliger, A. Urzhumtsev, P. H. Zwart, and P. D. Adams. 2012. Towards automated crystallographic structure refinement with phenix.refine. *Acta Crystallogr. D Biol. Crystallogr.* 68: 352–367.
25. Jones, T. A., J. Y. Zou, S. W. Cowan, and M. Kjeldgaard. 1991. Improved methods for building protein models in electron density maps and the location of errors in these models. *Acta Crystallogr. A* 47: 110–119.
26. Franke, D., A. G. Kikhney, and D. I. Svergun. 2012. Automated acquisition and analysis of small angle X-ray scattering data. *Nuclear Instruments and Methods in Physics Research Section A: Accelerators, Spectrometers, Detectors and Associated Equipment* 689: 52–59.
27. Petoukhov, M. V., P. V. Konarev, A. G. Kikhney, and D. I. Svergun. 2007. ATSAS 2.1 - towards automated and web-supported small-angle scattering data analysis. *J. Appl. Cryst.* 40: s223–s228.
28. Svergun, D., C. Barberato, and M. H. J. Koch. 1995. CRY SOL - A program to evaluate x-ray solution scattering of biological macromolecules from atomic coordinates. *J. Appl. Cryst.* 28: 768–773.
29. Szilágyi, A., Z. Bánlaki, E. Pozsonyi, E. J. Yunis, Z. L. Awdeh, A. Hossó, K. Rajczy, C. E. Larsen, D. A. Fici, C. A. Alper, and G. Füst. 2010. Frequent occurrence of conserved extended haplotypes (CEHs) in two Caucasian populations. *Mol. Immunol.* 47: 1899–1904.
30. Pan, Q., R. O. Ebanks, and D. E. Isenman. 2000. Two clusters of acidic amino acids near the NH2 terminus of complement component C4 alpha'-chain are important for C2 binding. *J. Immunol.* 165: 2518–2527.
31. van den Elsen, J. M., A. Martin, V. Wong, L. Clemenza, D. R. Rose, and D. E. Isenman. 2002. X-ray crystal structure of the C4d fragment of human complement component C4. *J. Mol. Biol.* 322: 1103–1115.
32. Duncan, R. C., F. Mohlin, D. Taleski, T. H. Coetzer, J. A. Huntington, R. J. Payne, A. M. Blom, R. N. Pike, and L. C. Wijeyewickrema. 2012. Identification of a catalytic exosite for complement component C4 on the serine protease domain of C1s. *J. Immunol.* 189: 2365–2373.
33. Dodds, A. W., X. D. Ren, A. C. Willis, and S. K. Law. 1996. The reaction mechanism of the internal thioester in the human complement component C4. *Nature* 379: 177–179.
34. Janatova, J., and B. F. Tack. 1981. Fourth component of human complement: studies of an amine-sensitive site comprised of a thiol component. *Biochemistry* 20: 2394–2402.
35. Chakravarti, D. N., R. D. Campbell, and R. R. Porter. 1987. The chemical structure of the C4d fragment of the human complement component C4. *Mol. Immunol.* 24: 1187–1197.
36. Morgan, H. P., C. Q. Schmidt, M. Guariento, B. S. Blaum, D. Gillespie, A. P. Herbert, D. Kavanagh, H. D. Mertens, D. I. Svergun, C. M. Johansson, et al. 2011. Structural basis for engagement by complement factor H of C3b on a self surface. *Nat. Struct. Mol. Biol.* 18: 463–470.
37. Kajander, T., M. J. Lehtinen, S. Hyvärinen, A. Bhattacharjee, E. Leung, D. E. Isenman, S. Meri, A. Goldman, and T. S. Jokiranta. 2011. Dual interaction of factor H with C3d and glycosaminoglycans in host-nonhost discrimination by complement. *Proc. Natl. Acad. Sci. USA* 108: 2897–2902.
38. Weiler, J. M. 1989. Regulation of C5 convertase activity by properdin, factors B and H. *Immunol. Res.* 8: 305–315.
39. Meri, S., and M. K. Pangburn. 1990. A mechanism of activation of the alternative complement pathway by the classical pathway: protection of C3b from inactivation by covalent attachment to C4b. *Eur. J. Immunol.* 20: 2555–2561.
40. Anderson, M. J., C. M. Milner, R. G. Cotton, and R. D. Campbell. 1992. The coding sequence of the hemolytically inactive C4A6 allotype of human complement component C4 reveals that a single arginine to tryptophan substitution at beta-chain residue 458 is the likely cause of the defect. *J. Immunol.* 148: 2795–2802.
41. McLean, R. H., G. Niblack, B. Julian, T. Wang, R. Wyatt, J. A. Phillips, III, T. S. Collins, J. Winkelstein, and D. Valle. 1994. Hemolytically inactive C4B complement allotype caused by a proline to leucine mutation in the C5-binding site. *J. Biol. Chem.* 269: 27727–27731.
42. Ebanks, R. O., and D. E. Isenman. 1995. Evidence for the involvement of arginine 462 and the flanking sequence of human C4 beta-chain in mediating C5 binding to the C4b subcomponent of the classical complement pathway C5 convertase. *J. Immunol.* 154: 2808–2820.
43. Hortin, G. L., T. C. Farries, J. P. Graham, and J. P. Atkinson. 1989. Sulfation of tyrosine residues increases activity of the fourth component of complement. *Proc. Natl. Acad. Sci. USA* 86: 1338–1342.
44. Janssen, B. J., A. Christodoulidou, A. McCarthy, J. D. Lambris, and P. Gros. 2006. Structure of C3b reveals conformational changes that underlie complement activity. *Nature* 444: 213–216.
45. Rodriguez, E., R. Nan, K. Li, J. Gor, and S. J. Perkins. 2015. A revised mechanism for the activation of complement C3 to C3b: a molecular explanation of a disease-associated polymorphism. *J. Biol. Chem.* 290: 2334–2350.
46. Wu, J., Y. Q. Wu, D. Ricklin, B. J. Janssen, J. D. Lambris, and P. Gros. 2009. Structure of complement fragment C3b-factor H and implications for host protection by complement regulators. *Nat. Immunol.* 10: 728–733.
47. Roversi, P., S. Johnson, J. J. Caesar, F. McLean, K. J. Leath, S. A. Tsiftoglou, B. P. Morgan, C. L. Harris, R. B. Sim, and S. M. Lea. 2011. Structures of the rat complement regulator CrrY. *Acta Crystallogr. Sect. F Struct. Biol. Cryst. Commun.* 67: 739–743.
48. Leung, E., A. M. Blom, L. Clemenza, and D. E. Isenman. 2006. The complement regulator C4b-binding protein (C4BP) interacts with both the C4c and C4dg subfragments of the parent C4b ligand: evidence for synergy in C4BP subsite binding. *Biochemistry* 45: 8378–8392.
49. Blom, A. M., A. F. Zadura, B. O. Villoutreix, and B. Dahlbäck. 2000. Positively charged amino acids at the interface between alpha-chain CCP1 and CCP2 of C4BP are required for regulation of the classical C3-convertase. *Mol. Immunol.* 37: 445–453.